Continuous self-assembly of organic–inorganic nanocomposite coatings that mimic nacre

Alan Sellinger*, Pilar M. Weiss*, Anh Nguyen*, Yunfeng Lu*, Roger A. Assink*, Weiliang Gong† & C. Jeffrey Brinker*

** Sandia National Laboratories and the University of New Mexico, NSF Center for Micro-Engineered Materials, The Advanced Materials Laboratory, 1001 University Blvd. SE, Albuquerque, New Mexico 87106, USA*
†Department of Earth and Planetary Sciences, The University of New Mexico, Albuquerque, New Mexico 87106, USA

Nanocomposite materials are widespread in biological systems. Perhaps the most studied is the nacre of abalone shell, an orientated coating composed of alternating layers of aragonite ($CaCO_3$) and a biopolymer. Its laminated structure simultaneously provides strength, hardness and toughness: containing about 1 vol. % polymer, nacre is twice as hard and 1,000 times as tough as its constituent phases[1]. Such remarkable properties have inspired chemists and materials scientists to develop synthetic, 'biomimetic' nanocomposite assemblies[2–5]. Nonetheless, the efficient processing of layered organic–inorganic composites remains an elusive goal. Here we report a rapid, efficient self-assembly process for preparing nanolaminated coatings that mimic the structure of nacre. Beginning with a solution of silica, surfactant and organic monomers, we rely on evaporation during dip-coating to induce the formation of micelles and partitioning of the organic constituents into the micellar interiors[6]. Subsequent self-assembly of the silica–surfactant–monomer micellar species into lyotropic mesophases[7] simultaneously organizes the organic and inorganic precursors into the desired nanolaminated form. Polymerization fixes this structure, completing the nanocomposite assembly process. This approach may be generalized both to other composite architectures and to other materials combinations.

Natural nanocomposites are formed by biomineralization[5], a templated self-assembly process in which pre-organized organic surfaces regulate the nucleation, growth, morphology and orientation of inorganic crystals. Related synthetic, so-called 'biomimetic', approaches include crystallization beneath Langmuir monolayers[8], crystallization on self-assembled monolayers[3,9], supramolecular self-assembly[2,6,10] and sequential deposition[11]. Of these, only the last two offer the ability to introduce periodic microstructural and compositional changes needed for nanocomposite assembly. With regard to nanolaminated structures, supramolecular self-assembly has resulted in the formation of lamellar (silica/surfactant) films[12] or

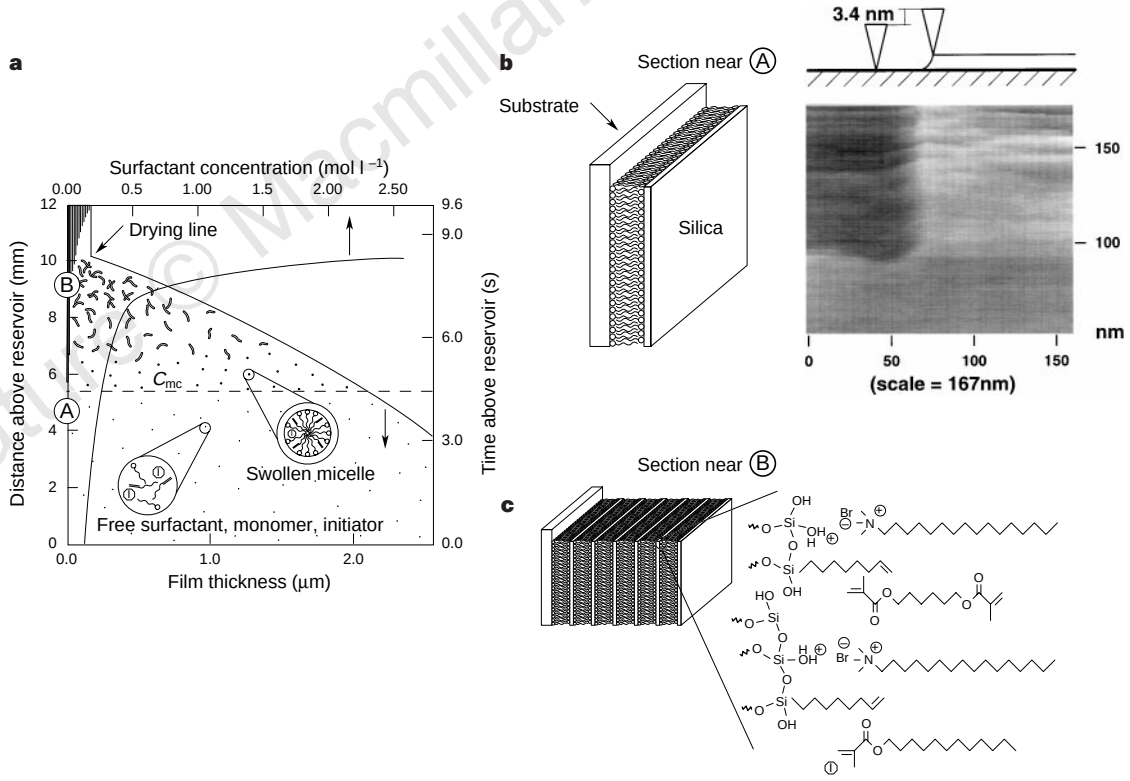

Figure 1 Diagrams showing evolution of nanolaminate structure during dip-coating (dip-coating rates ranged from 7.6 to 50.9 cm min^{-1}). **a**, Steady-state film-thinning profile established by evaporation, with vertical axes representing distance/time above sol reservoir surface, and horizontal axes showing film thickness and surfactant concentration. Preferential alcohol evaporation[25] progressively increases the surfactant concentration, inducing micellization and concurrent incorporation of monomer and initiator (I) into the micellar interior. **b**, Section near A. Surfactant bilayer formation occurs below c_{mc} and provides an organized surface for subsequent cooperative assembly of the lamellar mesophase. Bilayer structure was imaged using a non-contact AFM technique[26] following equilibration (1 h) of the silicon substrate with a silica–surfactant sol prepared with $c_0 = 5$ wt %, but without addition of organic monomer/initiator. Step height created by scraping the bilayer with the AFM tip is consistent with a CTAB bilayer[27]. **c**, Section near B showing the nanolaminate construction and hypothetical arrangement of surfactant, monomer, crosslinker and initiator adjacent to the oligomeric silicate surface. The chemical and structural characteristics of the coupling agent, monomers and initiators influence the local effective packing parameter of the surfactant and hence the organization of the hybrid mesophase[28]. In the present study it is possible that the organic monomers increase the effective volume of the surfactant chains stabilizing the lamellar mesophase[28].

multi-bilayer composite films[13], but such non-covalently bonded structures are mechanically unstable unless pillared[14] (for example, lamellar silica-surfactant coatings collapse to amorphous silica on surfactant removal[12]). Sequential deposition has been used to prepare stable inorganic/organic nanocomposites[11], but this process requires many repeated deposition steps to build up a practical coating thickness.

Our efficient assembly process for a poly(dodecylmethacrylate) (PDM)/silica nanocomposite is based on a simple dip-coating procedure[6] (see Fig. 1). The process starts with a homogeneous solution of soluble silicates, coupling agent, surfactant, organic monomers, and initiators prepared in ethanol/water solvent with an initial surfactant concentration (c_0) below the critical micelle concentration (c_{mc}). During dip-coating, preferential evaporation of ethanol progressively enriches the concentrations of water, HCl and the non-volatile solution constituents within the depositing film. Previous optical-probe experiments performed during dip-coating of related silica/surfactant/ethanol/water sols[6] indicated that the increasing concentrations of surfactant and water cause c to exceed c_{mc}, resulting in micelle formation and concurrent incorporation of hydrophobic optical probes into the micellar interiors. This evaporation-induced partitioning mechanism is used in the present study to incorporate alcohol soluble monomer(s) and initiators into micellar species. Continued evaporation promotes cooperative assembly of these (silica–surfactant–monomer) micellar species into interfacially organized liquid-crystalline mesophases, thereby simultaneously organizing both the inorganic and organic precursors into the desired laminated structure in a rapid (~10 s), continuous process. Organic polymerization (induced by light or heat), combined with continued inorganic polymerization, lock-in the nanocomposite architecture and covalently bond the organic–inorganic interface. Through variation of the surfactant type or its initial concentration, c_0, we can exploit supramolecular self-assembly to arrive at other nanocomposite constructions.

Precursor solutions were prepared by addition of cationic surfactant, organic monomer, crosslinker, initiator and unsaturated alkyltrialkoxysilane[15] (used in our study as a coupling agent) to an acidic silica sol (A2**). The acid concentration used in the A2** synthesis procedure was chosen to minimize the siloxane condensation rate[16], thereby promoting facile silica–surfactant supramolecular self-assembly during film deposition[6]. In a typical preparation, TEOS ($Si(OCH_2CH_3)_4$), ethanol (EtOH), water and dilute HCl (mole ratios: $1 : 3.8 : 1 : 5 \times 10^{-5}$) were heated at 60 °C for 90 min. The sol was diluted with ethanol (1 : 2) followed by addition of water and dilute HCl. Coupling agent (7-octenyltrimethoxysilane, OTS, or methacryloxypropyltrimethoxysilane, MPS) was added followed by surfactant (cetyltrimethylammonium bromide, CTAB), monomer (dodecylmethacrylate, DM), crosslinker (hexanedioldimethacrylate, HDM), and initiator (ultraviolet,

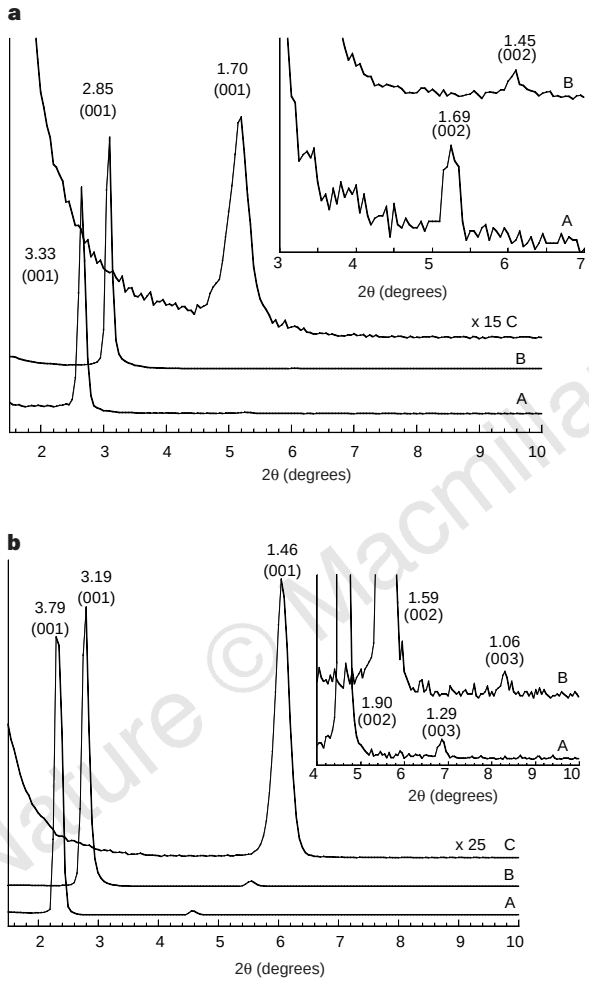

Figure 2 Thin film X-ray diffraction patterns of UV-initiated (**a**) and thermally-initiated (**b**) polymerization systems. Patterns were recorded on a Siemens D500 diffractometer using Ni-filtered CuKα radiation with $\lambda = 1.5418$ Å in θ–2θ scan mode. Traces A, as-deposited (unpolymerized); traces B, polymerized; and traces C, polymerized and washed. Traces A and B in panels **a** and **b** contain second-order reflections indicative of a lamellar liquid crystalline mesophase. **a**, On UV irradiation of A (Hg arc lamp source with filter providing wavelengths 260–320 nm and 20 mW cm^{-2} power density), a reduction in basal cell dimension of ~14% is observed (trace B), consistent with shrinkage in methacrylate-based polymerization systems[29]. An additional shrinkage of ~40% is observed following surfactant removal by washing in ethanol, acetone and diethylether (trace C). **b**, Thermal treatments of A (120 °C for 3 h) provide a reduction in basal cell dimension of ~16% (B), with an additional shrinkage of ~54% following surfactant removal (trace C). The increased shrinkage during polymerization and washing in the thermally initiated system (**b**) versus the UV-initiated system (**a**) results from the contribution of thermally induced silica polymerization and partial volatilization of monomer during thermal treatments.

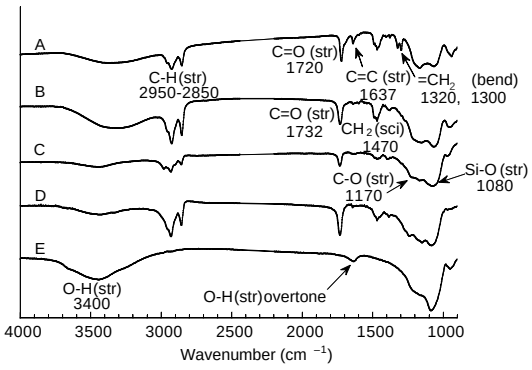

Figure 3 Fourier-transform infrared spectroscopy (FTIR) of nanocomposite coatings at various stages. Trace A, as-prepared (unpolymerized); trace B, polymerized (UV-irradiated); trace C, polymerized and washed; trace D, polymerized, washed, and treated in ammonium bifluoride to selectively etch the silica lamellae, and trace E, as-prepared and washed (without polymerization). Spectrum D contains all the bands of the bulk crosslinked PDM polymer plus siloxane bands due to the tri-functional siloxanes (coupling agents) that covalently bond the organic/inorganic interface and render the interfacial siloxane insoluble in NH_4HF_2. The importance of polymerization to lock in the structure is demonstrated in trace E where all monomer is lost if washed before UV irradiation. (Coatings were prepared on Petri dishes. Powders scraped from the substrate surface were dispersed in KBr pellets for IR analysis. Similar results were obtained from powders scraped off silicon substrates).

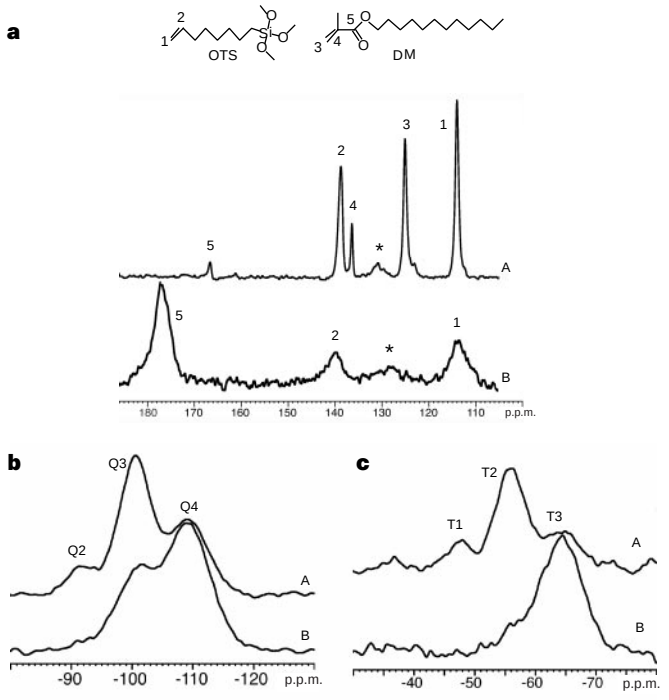

Figure 4 Magic-angle-spinning (MAS) solid-state NMR spectra of nanocomposite coatings. Trace A corresponds to as-prepared (unpolymerized), and B to polymerized (UV-irradiated), NH_3-treated, and washed samples. **a**, ^{13}C cross-polarization (CP) MAS spectra (100.6 MHz, 2 ms CP time, 1,024 scans) of the sp^2 hybridized region showing the disappearance of vinyl and methacrylate moieties of OTS and DM following polymerization (B). This demonstrates direct covalent linkages of DM to silica via vinyl-methacrylate group co-polymerization. The presence of residual vinyl resonances in B is not surprising as their reactivity is much less than that of methacrylates in this system. Residual peaks labelled with an asterisk probably correspond to DM polymer chain end groups derived from the aromatic carbons of the photo-initiator. **b**, ^{29}Si direct polarization MAS spectra (79.5 MHz, 240 s delay time, 128 scans) with extent of reaction values for A and B of 81.5% and 90.3%, respectively, calculated by deconvolution of the Q resonances (Q2/Q3/Q4 ratios change from 0.34/1.86/1.00 to 0/0.87/1.00). **c**, ^{29}Si CP-MAS spectra (79.5 MHz, 5 ms CP time, 1,024 scans) of the T region with extent of reaction values 68.2% and 95.5%, respectively, for A and B. Qn and Tn are tetrafunctional and trifunctional silanes, respectively, where n is a numeral corresponding to the number of bridging $\underline{Si}(OSi)_n$ groups surrounding the $\underline{Si}$ nucleus of interest. Samples prepared as in Fig. 3. Similar ^{13}C and ^{29}Si NMR results were obtained from the thermally initiated polymerization system.

benzoin dimethylether, BME; thermal, 1,1′-azobis(1-cyclohexanecarbonitrile, ACHN)). The final reactant mole ratios were: 1 TEOS:22 EtOH:5 H_2O:0.004 HCl:0.21 surfactant:0.16 DM:0.02 HDM:0.08 OTS:0.02 initiator. All materials are based on this formulation unless noted.

Coatings were deposited on polished, (100)-silicon by dip-coating (see Fig. 1). Thicker coatings required for spectroscopic measurements were prepared by dispensing a thin layer of sol in a Petri dish followed by immediate vertical draining. After deposition, the coatings were either heated or irradiated with ultraviolet light to initiate organic polymerization. Short exposures to ammonia vapour were used to promote further condensation of the silica framework. Polymerized coatings were washed sequentially with ethanol, acetone, and diethyl ether to remove surfactant and any unpolymerized species.

Figure 2 shows a typical series of X-ray diffraction (XRD) patterns corresponding to as-deposited (unpolymerized), polymerized and washed coatings for ultraviolet (Fig. 2a) and thermally-cured (Fig. 2b) systems. The XRD pattern of the as-deposited coating in Fig. 2a is consistent with a (001)-orientated lamellar phase with basal spacing $c = 3.33$ nm. The lamellar mesostructure is maintained during polymerization and washing, with associated basal spacing reductions of $c = 2.85$ and 1.70 nm, respectively. A similar trend is observed for the thermally initiated system. The first stage of shrinkage is due to both organic and inorganic polymerization (see following discussion) while that due to washing is a consequence of surfactant removal.

Figure 3 shows a series of Fourier-transform infrared (FTIR) spectra corresponding to the successive stages of nanocomposite formation for the ultraviolet-initiated polymerization system. Three features are observed that provide evidence of organic polymerization within the nanocomposite. (1) The C=C stretch (1,637 cm^{-1}) of the monomer and OTS virtually disappears after ultraviolet exposure, indicating C=C→C–C conversion. (2) The C=O stretching vibration in the unpolymerized film is shifted from 1,720 to 1,732 cm^{-1} after ultraviolet exposure, consistent with methacrylate polymerization[17] (conjugated versus unconjugated C=O stretch). (3) The bandwidth of the C=O-stretching peak in the polymerized film is narrower than that of low-molecular-weight polydodecylmethacrylate (PDM), suggesting that polymerization occurs within the confined geometry of the interlamellar galleries. Spectrum D in Fig. 3 is that of the polymer residue obtained after selectively etching the silica lamellae in ammonium bifluoride (NH_4HF_2). For wavenumbers greater than ~1,350 cm^{-1}, the spectrum is practically identical to that of the corresponding bulk crosslinked PDM. The presence of the Si–O stretching band in spectrum D is due to tri-functional siloxanes (T) (as confirmed by ^{29}Si magic-angle spinning (MAS) NMR) that covalently bond the inorganic/organic interface, rendering it insoluble in NH_4HF_2.

Further support for organic polymerization is found from ^{13}C NMR. As shown in Fig. 4a, the resonances at ~114–140 p.p.m. assigned to sp^2 hybridized carbons of $\underline{C}(CH_3)=\underline{C}H_2$ (DM) and $\underline{C}H=\underline{C}H_2$ (OTS) virtually disappear through conversion to sp^3 hybridization, and the $\underline{C}$=O resonance is shifted from 167 to 178 p.p.m., both indicative of methacrylate polymerization.

Evidence of inorganic polymerization is obtained from FTIR (see Fig. 3) and ^{29}Si MAS NMR (Fig. 4b, c). Integration of the envelope of peaks corresponding to the resonances of Q2, Q3 and Q4 silicon species shows that ammonia exposure causes the overall extent of siloxane condensation to increase from 80.2% to 88.4% and the extent of trisiloxane condensation (associated with the OTS coupling agent) to increase from 68.2% to 95.5%.

Nano-indentation measurements performed on PDM/silica, poly(4-methylstyrene)/silica and poly(4-vinylbenzylchloride)/silica nanolaminates prepared with ~50 wt% polymer show a three to seven times increase in indentation hardness (from 0.1–0.4 GPa to 0.8–1.0 GPa) due to combined organic/inorganic polymerization. We note that 1 GPa is the indentation hardness measured for rather dense sol–gel silica films.

The electron micrographs shown in Fig. 5 illustrate the diversity of structures attainable by this process. Figure 5a shows a transmission electron microscopy (TEM) image of a cross-section of the nanolaminated composite structure. Similar to shell, we observe a highly *c*-axis-orientated coating composed of successive layers of inorganic and organic polymers. Figure 5b shows a corresponding plan-view scanning electron microscopy (SEM) image, indicating that the nanocomposite coatings are featureless on micrometre length scales. Figure 5c shows a swirling pattern of organized tubules typical of hexagonal mesophases[2,18], and Fig. 5d shows a portion of a hierarchical composite coating composed of an isotropic worm-like micellar overlayer bonded to an orientated, nano-laminated underlayer.

Figure 5d provides support for formation mechanism depicted in Fig. 1. We propose that the lamellar structure originates from cooperative assembly of the swollen silica-surfactant micellar species with interfacially organized bilayers that form at the

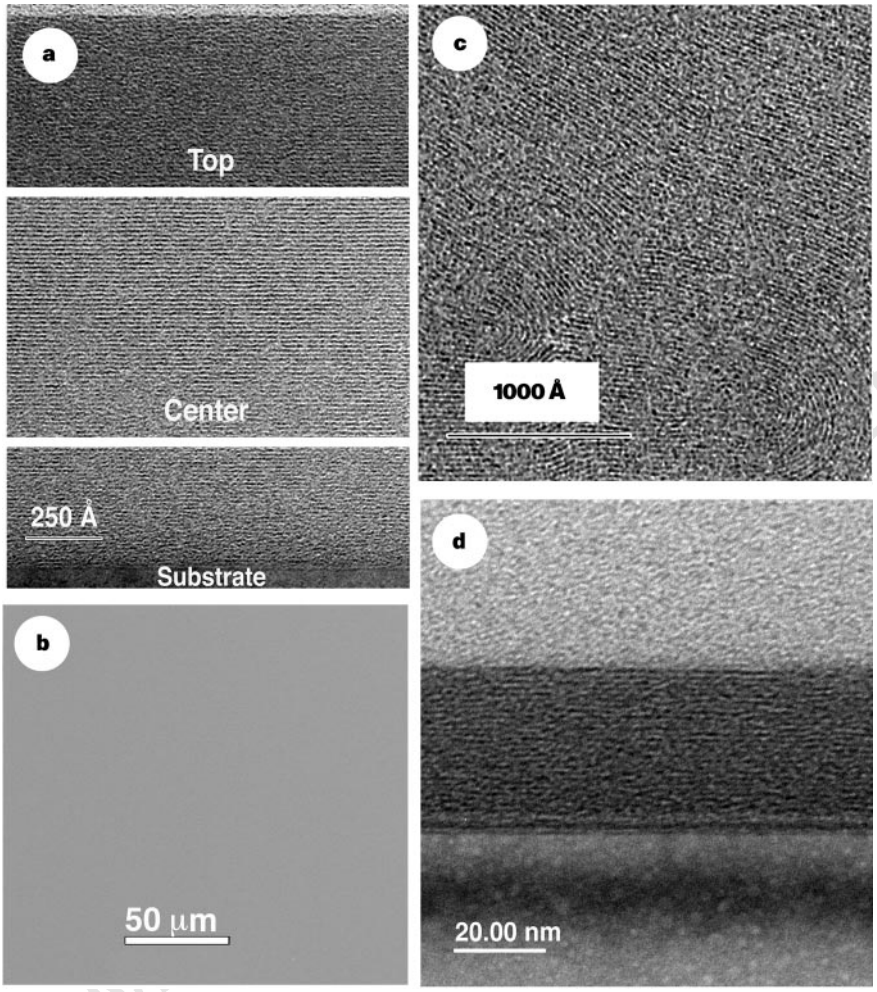

Figure 5 Electron micrographs of nanocomposite coatings prepared using the thermally initiated polymerization system ($c_0 = 5.0$ wt% CTAB) but with different coating rates or substrate surface treatments. All coatings were washed to remove surfactant and any unpolymerized species before sample preparation. **a**, TEM cross-section of ~500-nm-thick film showing *c*-axis-orientated nanolaminate structure. Shown are representative sections of the coating in the central region and regions adjacent to the substrate and vapour surfaces. (Coating prepared on KOH-treated silicon [100] substrate at withdrawal rate of 25.4 cm min^{-1}). **b**, SEM plan-view image of nanocomposite coating prepared as in **a**. All films appear featureless on this scale. **c**, TEM image of swirling pattern of tubules typical of hexagonal silica–surfactant mesophases formed at liquid–vapour or solid–liquid interfaces[2]. (Coating prepared as in **a** but at withdrawal rate of 12.7 cm min^{-1}). **d**, Cross-section of coating showing interface between ordered nanolaminate structure adjacent to silicon substrate and isotropic worm-like mesostructure. During film deposition, ordered lamellar regions appear to 'grow' from the substrate by a continuous, interfacially assisted self-assembly process[2,30]. The thickness of the ordered region depends on the process timescale (established by the coating rate) and the chemical nature of the substrate surface. (Film prepared as in **a** but with CTAB-treated surface).

solid–liquid interface at an earlier stage of the deposition process (as observed by atomic force microscopy (AFM), Fig. 1b). An ordered lamellar mesophase 'grows' from the substrate surface by continuous accretion. The thickness of the ordered region depends on c_0, the timescale of the dipping operation, and the chemical nature of the substrate surface.

Compared to sequential-deposition processes, the evaporation-induced partitioning and self-assembly inherent to our process allow simultaneous organization of the organic and inorganic precursors, so that thousands of layers form at once. In contrast to other nanocomposite self-assembly processes[19,21] we covalently link the organic and inorganic interface, and the continuous nature of our dip-coating process allows rapid formation of optically transparent coatings suitable for applications such as automotive finishes, hard coats, and optical hosts. The evaporation-induced partitioning approach is generally applicable to a wide range of organic and inorganic precursors, enabling the extension of this process to other materials combinations, such as inorganic/metal[22] or inorganic/conductive-polymer[23], of interest for high-capacitance devices, catalysis and quantum optics or electronics[24].

Received 19 February; accepted 13 May 1998.

1. Jackson, A., Vincent, J. & Turner, R. The mechanical design of nacre. *Proc. R. Soc. Lond. B* **234,** 415–425 (1988).
2. Aksay, I. *et al*. Biomimetic pathways for assembling inorganic thin films. *Science* **273,** 892–898 (1996).
3. Bunker, B. *et al*. Ceramic thin-film formation on functionalized interfaces through biomimetic processing. *Science* **264,** 48–55 (1994).
4. Heuer, A. *et al*. Innovative materials processing strategies: a biomimetric approach. *Science* **255,** 1098–1105 (1992).
5. Mann, S. Molecular tectonics in biomineralization and biomimetics materials chemistry. *Nature* **365,** 499–505 (1993).
6. Lu, Y. *et al*. Continuous formation of supported cubic and hexagonal mesoporous films by sol-gel dip-coating. *Nature* **389,** 364–368 (1997).
7. Kresge, C., Leonowicz, M., Roth, W., Vartuli, C. & Beck, J. Ordered mesoporous molecular sieves synthesized by a liquid-crystal template mechanism. *Nature* **359,** 710–712 (1992).
8. Heywood, B. & Mann, S. Template-directed nucleation and growth of inorganic materials. *Adv. Mater.* **6,** 9–19 (1994).
9. Tarasevich, B., Rieke, P. & Liu, J. Nucleation and growth of oriented ceramic films onto organic interfaces. *Chem. Mater.* **8,** 292–300 (1996).
10. Yang, H., Kuperman, A., Coombs, N., Mamiche-Afara, S., Ozin, G. Synthesis of oriented films of mesoporous silica on mica. *Nature* **379,** 703–705 (1996).
11. Keller, S., Kim, H. & Mallouk, T. Layer-by-layer assembly of intercalation compounds and heterostructures on surfaces: toward molecular "beaker" epitaxy. *J. Am. Chem. Soc.* **116,** 8817–8818 (1994).
12. Ogawa, M. Formation of novel oriented transparent films of layered silica-surfactant nanocomposites. *J. Am. Chem. Soc.* **116,** 7941–7942 (1994).
13. Okada, H., Sakata, K. & Kunitake, T. Formation of oriented iron oxide particles in cast multibilayer films. *Chem. Mater.* **2,** 91–93 (1990).

14. Tanev, P. & Pinnavaia, T. Biomimetic templating of porous lamellar silicas by vesicular surfactant assemblies. *Science* **271** 1267–1269 (1996).
15. Burkett, S., Sims, S. & Mann, S. Synthesis of hybrid inorganic-organic mesoporous silica by co-condensation of siloxane and organosiloxane precursors. *Chem. Commun.* **11,** 1367–1368 (1996).
16. Brinker, C., Sehgal, R., Raman, N., Schunk, P. & Headley, T. Polymer approach to supported silica membranes. *J. Sol-Gel Sci. Technol.* **2,** 469–476 (1994).
17. Pretsch, E., Siebl, J., Simon, W. & Clerc, T. in *Tables of Spectral Data for Structure Determination of Organic Compounds* (eds Pretsch, E., Siebl, J., Simon, W. & Clerc, T.) I141–I142 (Springer, Berlin, 1989).
18. Yang, H., Coombs, N., Dag, O., Sokolov, I. & Ozin, G. Free-standing mesoporous silica films; morphogenesis of channel and surface patterns. *J. Mater. Chem.* **7,** 1755–1761 (1997).
19. Giannelis, E. Polymer layered silicate nanocomposites. *Adv. Mater.* **8,** 29–35 (1996).
20. Gray, D., Hu, S., Juang, E. & Gin, D. Highly ordered polymer-inorganic nanocomposites via monomer self-assembly: in situ condensation approach. *Adv. Mater.* **9,** 731–736 (1997).
21. Templin, M. *et al.* Organically-modified aluminosilicate mesostructures from block-copolymer phases. *Science* **278,** 1795–1798 (1997).
22. Huber, C., Moller, K. & Bein, T. Reactivity of a trimethylstannyl molybdenum complex in mesoporous MCM-41. *J. Chem. Soc.* 2619–2620 (1994).
23. Wu, C. & Bein, T. Conducting polyaniline filaments in a mesoporous channel host. *Science* **264,** 1757–1759 (1994).
24. Ozin, G. Nanochemistry: synthesis in diminishing dimensions. *Adv. Mater.* **4,** 612–649 (1992).
25. Nishida, F. *et al.* In situ fluorescence probing of the chemical changes during sol-gel thin film formation. *J. Am. Ceram. Soc.* **78,** 1640–1648 (1995).
26. Manne, S., Cleveland, J., Gaub, H., Stucky, G. & Hansma, P. Direct visualization of the surfactant hemimicelles by force microscopy of the electrical double layer. *Langmuir* **10,** 4409–4413 (1994).
27. Bull, L. *et al.* in *Zeolites and Related Microporous Materials: State of the Art 1994* (eds Weitkamp, J., Karge, H., Pfeifer, H. & Holderich, W.) 429–434 (Elsevier, Amsterdam, 1994).
28. Israelachvili, J. *Intermolecular and Surface Forces* (Academic, San Diego, 1992).
29. Odian, G. *Principles of Polymerization* (Wiley, New York, 1981).
30. Yang, H., Coombs, N., Sokolov, I. & Ozin, G. Free-standing and oriented mesoporous silica films grown at the air-water interface. *Nature* **381,** 589–592 (1996).

Acknowledgements. We thank S. Singh, R. Tissot, S. Rao, Y. Guo and D. Schmale for assistance with experimental portions of this work, and M. Aragon and K. Burns for technical illustrations. This work was supported in part by the UNM/NSF Center for Micro-Engineered Materials, DOE Basic Energy Sciences, and SNL's Laboratory-Directed Research and Development Program (LDRD); and by the US Department of Energy. Sandia is a multiprogram laboratory operated by Sandia Corporation, a Lockheed Martin Company, for the US Department of Energy.

Correspondence and requests for materials should be addressed to C.J.B. (e-mail: cjbrink@sandia.gov).

Rapid eruption of Skye lavas inferred from precise U–Pb and Ar–Ar dating of the Rum and Cuillin plutonic complexes

M. A. Hamilton*, D. G. Pearson†, R. N. Thompson†, S. P. Kelley‡ & C. H. Emeleus†

** Continental Geoscience Division, Geological Survey of Canada, Ontario, Canada K1A 0E8*
† Department of Geological Sciences, Durham University, South Road, Durham DH1 3LE, UK
‡ Department of Earth Sciences, The Open University, Milton Keynes, MK7 6AA, UK

The interpretation of rocks of the British Tertiary Volcanic Province has played an important role in the historical development of many concepts in igneous petrology. Exposures of lavas, sub-volcanic rocks and plutonic complexes have allowed a detailed understanding of the field relationships between such units in the context of flood-basalt magmatism[1–3]. Nevertheless, age control has been a source of much controversy and a limiting factor in comparing these relationships to recent developments in the theoretical modelling of magmatism within continents[4]. Here we report precise $^{206}Pb/^{238}U$ zircon ages of 60.53 ± 0.08 Myr (2σ) for the Rum basic/ultrabasic pluton and 58.91 ± 0.07 Myr for the Cuillin gabbros, Skye, which tightly constrain eruption of the greater than 1.5-km-thick Skye lavas to a maximum duration of 1.6 ± 0.2 Myr. These dates yield magma production rates for the Skye lavas of about 2.2×10^{-3} km^3 yr^{-1} comparable with rates inferred for individual magmatic centres produced by melting related to mantle plumes below ocean basins. In addition, the approximately 30 km of lithospheric thinning suggested by magma chemistry is required to have occurred in less than 2 Myr.

The >1.5-km-thick Skye main lava succession (SMLS)[5–7] is the remnant of an important surface expression of the magmatism related to rifting of the northeast Atlantic continental margin due to impingement of the Iceland mantle plume 63 Myr ago[8,9]. Geochemical studies on Skye lavas show that they are dominated by transitional to alkali-basalts of the SMLS[2,10]. A later, tholeiitic magma type, Preshal-More basalt, was produced in large volumes but is now mostly preserved as dykes[11]. Flows of Preshal-More basalts overlie the SMLS and have compositions more akin to mid-ocean-ridge basalt (MORB). The temporal change in major- and trace-element composition between the SMLS and Preshal-More magma types[12] has been interpreted in terms of progressive lithospheric thinning beneath Skye[13]. Determination of the timespan of lava eruptions will

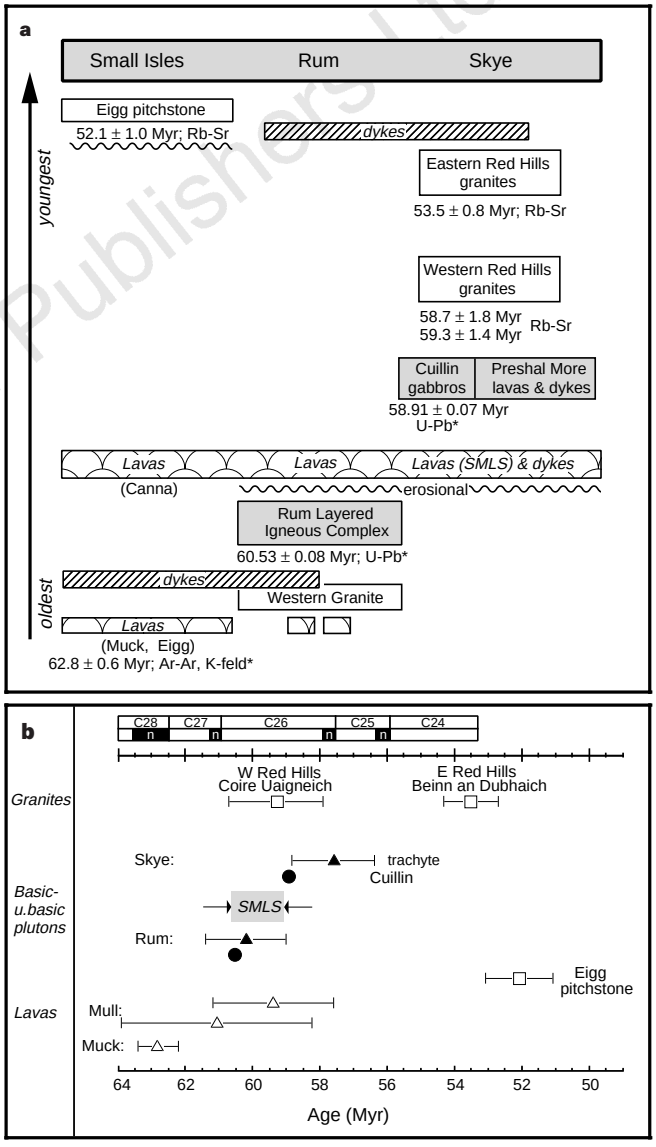

Figure 1 Field and chronostratigraphy of magmatism on Rum, Skye and the Small Isles. **a**, Diagrammatic representation of simplified igneous stratigraphical relationships established on the basis of field relations (see ref. 3 for summary). Radioisotopic ages are given with method; asterisk shows new dates; shown are data from this work and ref. 8; errors are 2σ. For a more comprehensive summary of ages and their source see ref. 9. **b**, Comparison of Rum-Skye basic/ultrabasic complex U–Pb zircon ages with other ages for Skye igneous events and Mull, Muck and Eigg lava suites. Squares indicate Rb–Sr isochrons, triangles are $^{40}Ar/^{39}Ar$ step heating ages, and circles are U–Pb zircon ages; filled symbols are data from this study. For sources of dates see Table 1 and refs 3, 8, 9, 17, 25. Arrows indicate 2σ uncertainties in all cases. Chronostratigraphic timescale is from ref. 26. Maximum likely duration of Skye lavas (SMLS) shown by shading.